International Forum on Aeroelasticity and Structural Dynamics
IFASD 2017
25-28 June 2017 Como, Italy

RESEARCH ON FAST AEROELASTIC MODELING METHODS FOR THE TRANSONIC REGIME

Hüseyin Güner, Grigorios Dimitriadis, Vincent E. Terrapon

Department of Aerospace and Mechanical Engineering, B52/3
University of Liège
B-4000 Liège, Belgium
hguner@ulg.ac.be
gdimitriadis@ulg.ac.be
Vincent.Terrapon@ulg.ac.be

Keywords: Transonic flow, unsteady aerodynamics modeling, computational fluid dynamics, dynamic mode decomposition, harmonic balance method, aeroelasticity.

Abstract: Two methods for modeling unsteady transonic flows at low computational cost are presented as a first step towards a fast and accurate aeroelastic calculation methodology for the preliminary design stage in the transonic flow regime. The first approach corresponds to a quasi-steady approximation based on few steady simulations that is improved through the use of an unsteady filter. The second approach is based on the interpolation of dynamic modes between solutions at different frequencies that are obtained either from Dynamic Mode Decomposition (DMD) of unsteady simulations or directly from Harmonic Balance (HB) simulations. The two methods are illustrated in the case of a pitching airfoil in the transonic regime. Results show that the first method is fast and provides a first approximation of the unsteady dynamics. The computational cost of the second approach is higher, but the method provides better results in predicting aerodynamic forces and shock motion for a large range of reduced frequencies.

1 INTRODUCTION

The prediction of transonic flutter is of great importance to aircraft design as transport aircraft commonly cruise in the transonic flow regime. Some supersonic aircraft must also be designed to fly at transonic conditions during specific phases of their mission. However, the computation of the aeroelastic response of aircraft wings or control surfaces is challenging in this regime because unsteady transonic flows are characterized by aerodynamic nonlinearities such as moving shock waves and shock-boundary layer interactions. These nonlinear phenomena can result in unwanted aeroelastic effects including Limit Cycle Oscillations (LCOs), and limit the performance of aircraft [1, 2].

The aerospace industry relies on unsteady panel methods based on the linearized potential equation, such as the Doublet-Lattice Method (DLM) [3], for routine aeroelastic analyses. Although these linear codes provide rapid and accurate predictions of the aerodynamic loads for purely subsonic or supersonic flows, they cannot capture the critical unsteady phenomena present in transonic flows (e.g., shock oscillations). This type of flow being inherently nonlinear, the full potential equation cannot be linearized even for small perturbations, and the aeroelastic calculations require higher-fidelity approaches.

Driven by the advance in computing power, different approaches have been proposed based on the Transonic Small Disturbance (TSD) equation, the full potential equation, the inviscid Euler equations, or the Reynolds-Averaged Navier-Stokes (RANS) equations [1]. At the present time, the best option to accurately account for unsteady nonlinear phenomena is to rely on the Euler or RANS equations. However, the use of Euler or RANS codes in industrial aeroelastic applications is limited due to the high computational cost required for repeated unsteady simulations. Another approach currently available is the field-panel method based on the Time-Linearized Transonic Small Disturbance (TLTSD) equation [4], which models the flow as a linear time-varying perturbation around a mean nonlinear steady solution. The major shortcoming of this method is that it precludes large unsteady disturbances, i.e., the shocks cannot oscillate and the boundary layers cannot feature significant unsteadiness.

The overall objective of this work is to develop a novel unsteady aerodynamic modeling methodology with higher fidelity than the linear panel approaches, especially at transonic conditions, and with a computational cost that is low enough to be applied to aeroelastic tailoring problems.

The present study proposes two approaches as a first step towards this objective. It focuses on the computation of the transonic flow around a pitching airfoil. This configuration has been chosen because it enables the study of shocks that move due to structural oscillations. Section 3 presents the reference case and the time-accurate Euler solutions, which will be used for validation purposes.

The first proposed approach introduced in Section 4 relies on a few steady results calculated by solving the steady Euler equations. However, the steady flow fields are clearly different from the unsteady ones, and a filtering technique is suggested to improve the steady estimations.

The second approach presented in Section 5 is based on the interpolation of a few Dynamic Mode Decomposition (DMD) [5, 6] modes, obtained from the decomposition of the results of unsteady Euler simulations. The motivation is to develop a methodology that accounts for the unsteady nonlinear aerodynamic effects more accurately for a large range of frequencies. Moreover, an unsteady Euler simulation being computationally expensive for practical applications, the Harmonic Balance (HB) [7,8] method is suggested as an efficient alternative for calculating the dynamic modes. An overview of the existing numerical methods used in the present study is presented in the next section.

2 NUMERICAL METHODS

2.1 Time-accurate simulation

All numerical simulations are performed with the open-source CFD code SU2 [9]. This solver is based on a finite volume discretization and a dual time-stepping time integration to solve the Euler or RANS equations.

2.2 Dynamic mode decomposition

The unsteady flow fields are processed using the Dynamic Mode Decomposition (DMD) [5, 6, 10] in order to extract information about the flow dynamics. DMD is applied to a sequence of N flow fields represented by a matrix $\mathbf{V}_1^N$:

$$\mathbf{V}_1^N = \{\mathbf{v}_1, \mathbf{v}_2, \mathbf{v}_3, \ldots, \mathbf{v}_N\}, \tag{1}$$

where $\mathbf{v}_n$ is a vector corresponding to the nth flow field. Two consecutive snapshots $\mathbf{v}_n$ and $\mathbf{v}_{n+1}$ are assumed to be separated by a constant time step Δt that must be small enough so that the relevant dynamic processes can be extracted from the input data sequence.

The application of the DMD procedure results in $N-1$ modes, which consist of the eigenvalues λ_i, the modal amplitudes α_i, and the mode shapes $\boldsymbol{\phi}_i$ such that

$$\mathbf{v}_n = \sum_{i=1}^{N-1} \alpha_i \boldsymbol{\phi}_i \mathrm{e}^{\lambda_i (n-1)\Delta t}, \qquad n \in \{1, 2, 3, \ldots, N-1\}. \tag{2}$$

The growth/decay rates and frequencies of the individual modes are respectively the real and imaginary parts of λ_i.

2.3 Harmonic balance method

The Harmonic Balance (HB) method [7, 8] solves the governing equations for a specified set of frequencies

$$\boldsymbol{\omega} = \begin{bmatrix} \omega_0 & \omega_1 & \omega_2 & \ldots & \omega_K & \omega_{-K} & \ldots & \omega_{-1} \end{bmatrix}^{\mathrm{T}}, \tag{3}$$

where $\omega_0 = 0$, $\omega_{-i} = -\omega_i$, and K is the number of specified frequencies. In general, the HB method can be used for flows with several fundamental frequencies, and so the discrete frequencies are not necessarily multiples of each other. The period T of HB simulation is divided into $N = 2K + 1$ time instances. In the case where the flow problem contains multiple fundamental frequencies, T can be calculated by the algorithm given in [11].

A Fourier representation of each conservation variable is written using the period and the set of frequencies:

$$\hat{\varphi}_k = \frac{1}{N} \sum_{n=0}^{N-1} \varphi_n \mathrm{e}^{-i\omega_k t_n}, \tag{4}$$

or in matrix form using the discrete Fourier transform matrix E:

$$\hat{\boldsymbol{\varphi}} = E\boldsymbol{\varphi}^*, \qquad E_{k,n} = \frac{1}{N} \mathrm{e}^{-i\omega_k t_n}, \tag{5}$$

where

- $\boldsymbol{\varphi}^* = \begin{bmatrix} \varphi_0 & \varphi_1 & \varphi_2 & \ldots & \varphi_{N-1} \end{bmatrix}^{\mathrm{T}}$ represents a single conservation variable at the N time instances throughout the period $t_n = (n-1)T/N$.
- $\hat{\boldsymbol{\varphi}} = \begin{bmatrix} \hat{\varphi}_0 & \hat{\varphi}_1 & \hat{\varphi}_2 & \ldots & \hat{\varphi}_K & \hat{\varphi}_{-K} & \ldots & \hat{\varphi}_{-1} \end{bmatrix}^{\mathrm{T}}$ is the vector of Fourier coefficients in the frequency domain.

Applying the time derivative operator to $\boldsymbol{\varphi}^*$ gives

$$D_t \boldsymbol{\varphi}^* = D_t(E^{-1}\hat{\boldsymbol{\varphi}}) = \frac{\partial E^{-1}}{\partial t}\hat{\boldsymbol{\varphi}} = \frac{\partial E^{-1}}{\partial t} E\boldsymbol{\varphi}^*, \tag{6}$$

and therefore

$$D_t = \frac{\partial E^{-1}}{\partial t} E. \tag{7}$$

If the system has only one fundamental frequency, the discrete frequencies are given by $\omega_k = k2\pi/T$ and the inverse Fourier transform E^{-1} has the analytic expression

$$E^{-1}_{n,k} = \mathrm{e}^{i\omega_k t_n}. \tag{8}$$

Otherwise, it is easier to first write an analytical expression directly for E^{-1} to determine its derivative, and calculate E by numerically inverting E^{-1} [11].

The formulation leads to a system of coupled steady simulations that are solved simultaneously by marching in time towards steady state.

3 REFERENCE CASE

The reference case consists in the calculation of the 2D transonic flow over a NACA 64A010 airfoil, shown in Figure 1(a), pitching about its quarter-chord point. In the experiment by Davis [12], the free-stream Mach number M_∞ is 0.796 and the Reynolds number, Re, based on the chord c is 12.56×10^6. The pitching motion is specified as

$$\alpha(\tau) = \alpha_m + \alpha_0 \sin(k\tau) \tag{9}$$

$$= 0^\circ + 1.01^\circ \sin(0.202\tau), \tag{10}$$

where $\alpha(\tau)$ is the variation of the angle of attack with non-dimensional time $\tau = tU_\infty/b$, U_∞ is the free-stream velocity, $b = c/2$, α_m is the mean angle of attack, α_0 is the pitching amplitude, and the reduced frequency is defined as $k = \omega b/U_\infty = 0.202$ with ω the angular frequency. Because the maximum pitch angle is small, the flow remains attached.

3.1 Time-accurate Euler solution

In the present study, only two-dimensional Euler simulations are considered. A C-type grid is generated around the airfoil, as shown in Figure 1(b). The grid has about 29,500 quadrilaterals with 300 points around the airfoil. The boundaries of the computational domain are located about $50c$ away from the airfoil in order to minimize their impact on the solution in the region of interest. The time-accurate simulation uses 25 time steps per period of oscillation to capture the relevant time scales, and the calculation is run until a periodic state has been reached to eliminate transient effects.

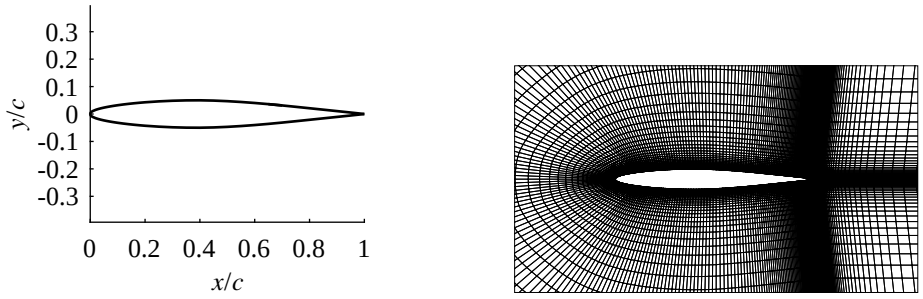

(a) Airfoil shape. (b) Grid.

Figure 1: NACA 64A010 airfoil shape and close-up view of the grid around the airfoil for Euler simulations.

Figure 2 shows that the variation of the lift coefficient, c_l, and the chordwise position of the shock on the upper surface, x_s, obtained by the unsteady Euler simulation are in agreement

with the experimental measurements for the reference conditions. Although convergence acceleration techniques available for steady-state problems can be used with a dual time-stepping approach, time-accurate simulations remain computationally expensive. In particular, the calculation of transients consumes a significant part of the computational time.

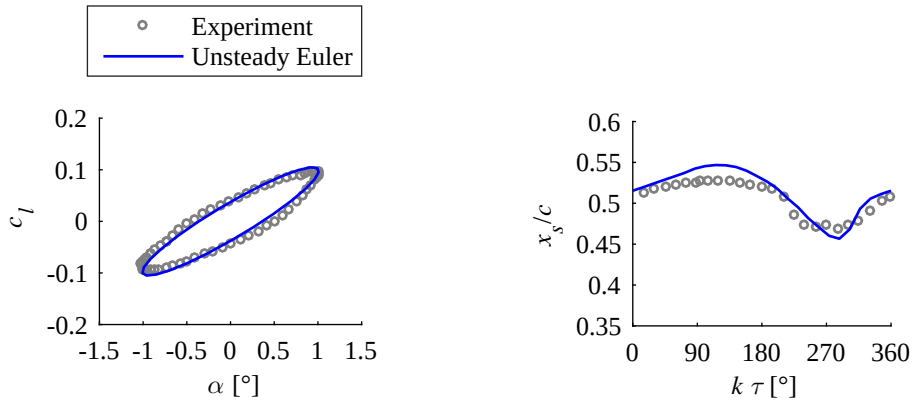

(a) Lift coefficient.

(b) Shock position.

Figure 2: Variation of lift coefficient and position of the shock on the upper surface of the airfoil over one oscillation cycle, $k = 0.202$.

4 APPROACH USING A FEW STEADY SOLUTIONS

The present section focuses on using a small number of steady Euler simulations and applying a filter to estimate the unsteady flow around the pitching airfoil. First, the approach is demonstrated on the time response of the Mach field. Then, the shock motion is considered as a quantitative comparison to the unsteady Euler simulation results for a large range of reduced frequencies.

4.1 Mach field

The first row of Figure 3 represents three snapshots of the Mach field $M(x, y, \tau)$ at three instantaneous phase angles computed by an unsteady Euler simulation of the reference case, for $k = 0.202$. The shocks lie at the edge of the supersonic regions and their position clearly varies over time. The shock on the upper surface moves downstream and becomes stronger during the upstroke. The opposite happens during the downstroke; the shock on the upper surface moves upstream and becomes weaker. The same behavior is observed on the lower surface with a half-period lag, as the configuration is symmetric.

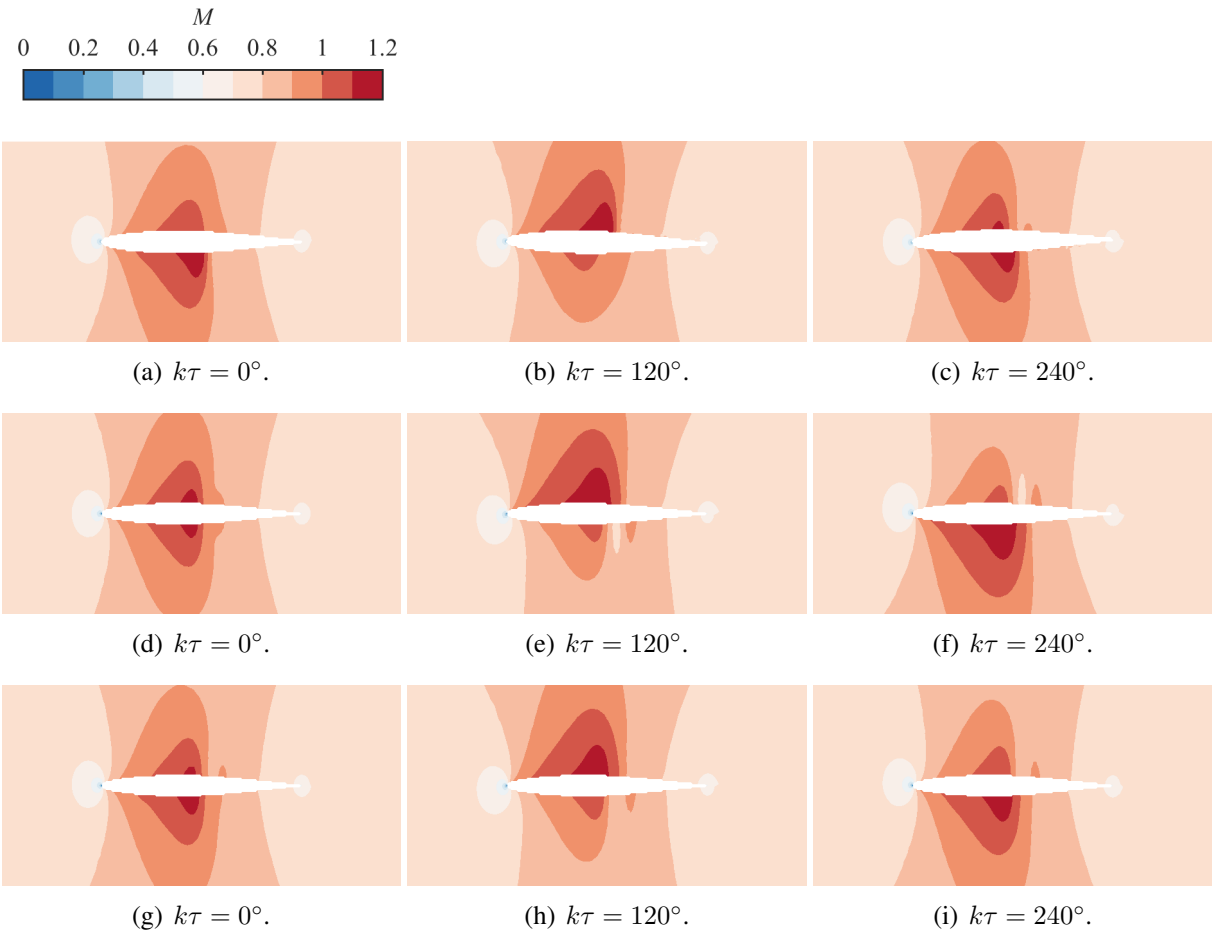

(a) $k\tau = 0°$. (b) $k\tau = 120°$. (c) $k\tau = 240°$.

(d) $k\tau = 0°$. (e) $k\tau = 120°$. (f) $k\tau = 240°$.

(g) $k\tau = 0°$. (h) $k\tau = 120°$. (i) $k\tau = 240°$.

Figure 3: Mach contours at different phases of the oscillation cycle obtained by (a–c) an unsteady Euler simulation, (d–f) using steady Euler solutions, and (g-i) applying Theodorsen's filter to steady Euler solutions.

The second row of Figure 3 depicts snapshots at the same instantaneous angles obtained through a quasi-steady approximation. In particular, two steady Euler simulations are used to determine the mean field at the mean angle of attack, and the derivative of this field with respect to alpha. In the context of this quasi-steady approximation, the time response of the Mach number field can be expressed as

$$M_{qs}(x, y, \tau) = M(x, y, \alpha = \alpha_m) + \frac{\partial M(x, y, \alpha = \alpha_m)}{\partial \alpha}(\alpha(\tau) - \alpha_m). \tag{11}$$

In this case, the two steady simulations have been performed at the mean angle of attack and at the maximum pitching amplitude.

When $k\tau = 0°(\alpha = 0°)$, it can be seen that the lower and upper parts of the Mach field are not symmetrical for the unsteady case, while the steady simulation at this angle of attack provides a symmetrical solution, which is expected from the symmetry of the airfoil. When $k\tau = 120°$ ($\alpha \approx 0.87°$), the quasi-steady calculation overestimates the extent of the supersonic region on the upper part and underestimates its size on the lower part.

A quasi-steady approach is tempting because of its low computational cost and independence with respect to the reduced frequency, but the resulting Mach field predictions, and hence shock motions, are inaccurate. More representative results can be obtained by applying an unsteady filter to Equation (11). As a simple example, Theodorsen's function $C(k)$ [13] is considered (see Figure 4). The function $C(k)$ can be seen as an analog filter since its amplitude decreases with k, tending to 0.5 as k tends to infinity. Equation (11) becomes

$$M_f(x, y, \tau) = M(x, y, \alpha = \alpha_m) + \frac{\partial M(x, y, \alpha = \alpha_m)}{\partial \alpha}\Im(C(\bar{k})\alpha_0 \mathrm{e}^{ik\tau}), \tag{12}$$

where $\bar{k} = \omega b/(\beta U_\infty)$ and $\beta = \sqrt{1 - M_\infty^2}$.

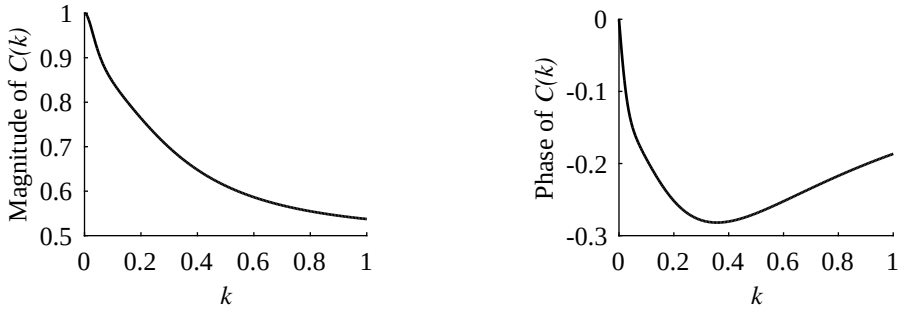

(a) (b)

Figure 4: (a) Magnitude and (b) phase angle of Theodorsen's function as a function of the reduced frequency.

The third row of Figure 3 shows the results computed by the filtered quasi-steady technique. At $k\tau = 0°$, the filter introduces a dissymmetry in the field compared to the steady case, which is qualitatively closer to the unsteady case. At $k\tau = 120°$, the filter reduces the supersonic region on the upper part obtained by the steady case, and thus provides a better approximation to the unsteady case. Nonetheless, discrepancies with the unsteady Euler solution are still present.

4.2 Shock motion

A supersonic flow is decelerated to subsonic through a shock wave. Therefore, a shock lying on the airfoil can be extracted directly from the Mach field of an inviscid flow. Applying the

idea of the quasi-steady analysis, the two steady simulations can be used to determine the mean shock position, x_m, and the amplitude of the shock motion, x_0, such that

$$x_s(\tau) = x_m + x_0 \sin k\tau. \tag{13}$$

Theodorsen's filter corrected for compressibility can again be applied in order to improve the quasi-steady approximation, such that

$$x_s(\tau) = x_m + \Im(C(\bar{k})x_0 \mathrm{e}^{ik\tau}). \tag{14}$$

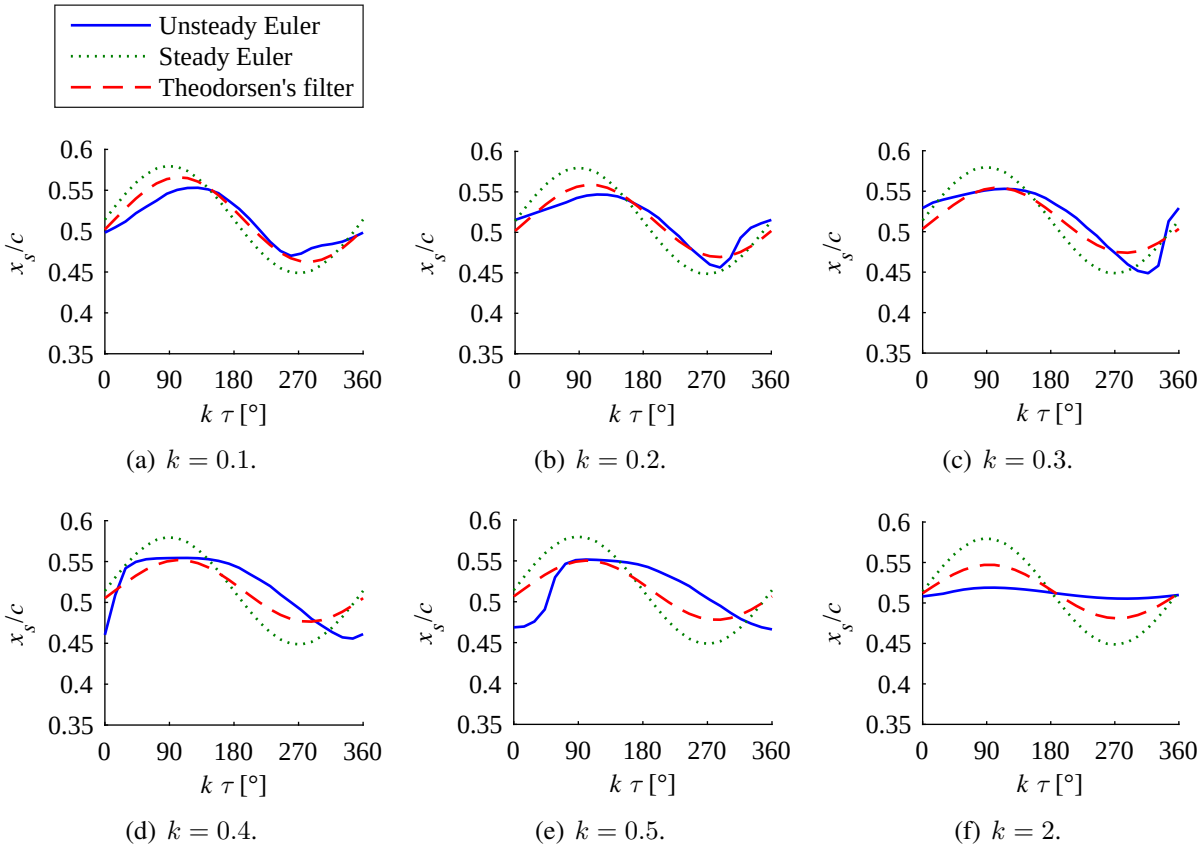

(a) $k = 0.1$. (b) $k = 0.2$. (c) $k = 0.3$.

(d) $k = 0.4$. (e) $k = 0.5$. (f) $k = 2$.

Figure 5: Influence of the reduced frequency on the shock motion on the upper surface of the airfoil.

Figure 5 repeats the analysis performed for the reference case to different values of the reduced frequency. It shows that the filtered quasi-steady approach provides acceptable results when k is below 0.4, which is promising knowing that the reduced frequency at flutter is typically of the order of 0.1 for most transonic flutter problems encountered in aircraft wings or control surfaces [1]. For higher frequencies, the predicted unsteady shock motion becomes more irregular, and this behavior cannot be fully recovered by applying the filter. On the other hand, when k is very large ($k = 2$), the shock motion is negligible.

The basic Theodorsen's function depends on the oscillation frequency. More specifically, applying Theodorsen's filter cannot predict higher harmonics, which partly explains the discrepancies observed with the exact unsteady solution. Better results could potentially be obtained with a different filter that includes harmonics. The contribution of higher harmonics is discussed in the next section.

5 APPROACH USING A FEW DMD MODES

Before presenting the second proposed methodology, flow fields obtained from unsteady Euler simulations at different pitching frequencies are first processed using Dynamic Mode Decomposition (DMD) in order to extract information about the flow dynamics. More specifically, a DMD analysis generates dynamic modes oscillating at a single frequency, allowing a better description of the influence of the reduced frequency on the transonic flow around the pitching airfoil.

5.1 Dynamic mode decomposition analyses

DMD is applied to the Mach fields generated by the unsteady Euler simulations for three reduced frequencies $k = 0.1, 0.3$, and 0.5. The spatial size of the snapshots is chosen large enough to include the supersonic regions, and 25 snapshots are taken per period. Figure 6 plots the resulting modal amplitudes α_i against the corresponding modal reduced frequencies $\Im(\lambda_i)b/U_\infty$ for the simulations carried out at the three values of k. Each DMD amplitude distribution is discrete and symmetrical with respect to $\Im(\lambda_i) = 0$ because the input data are real [5]. The modes are sorted by descending amplitude. The highest peak represents the contribution of the mean flow, which is constant over time ($\Im(\lambda_0) = 0$).

A peak appears at the fundamental frequency, which corresponds to the imposed pitching frequency, such that $\Im(\lambda_1)b/U_\infty = k$. The harmonics (i.e., integer multiples of the fundamental frequency) are well distinguishable, even at high k, but their amplitude decreases with $\Im(\lambda_i)b/U_\infty$. Therefore, the modes at high $\Im(\lambda_i)b/U_\infty$ make a relatively small contribution to the dynamics of the system.

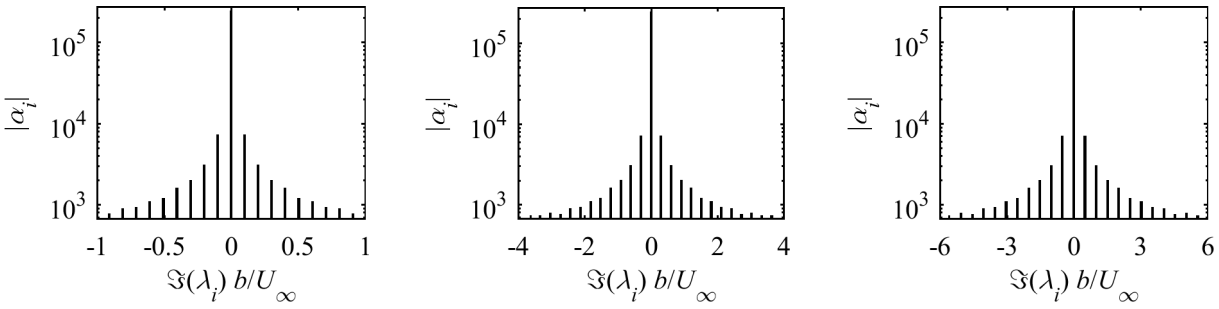

(a) $k = 0.1$. (b) $k = 0.3$. (c) $k = 0.5$.

Figure 6: Absolute value of the DMD amplitude as a function of non-dimensional frequency in a semilogarithmic plot.

Figure 7 plots the shape $\alpha_0\boldsymbol{\phi}_0$ of mode zero, i.e., the mean flow, as calculated from three unsteady simulations at $k = 0.1, 0.3$, and 0.5. It shows that the DMD representation of the mean flow does not vary with reduced frequency for these cases. Note that the oscillations have small amplitude, separated flow cases would not necessarily lead to the same result.

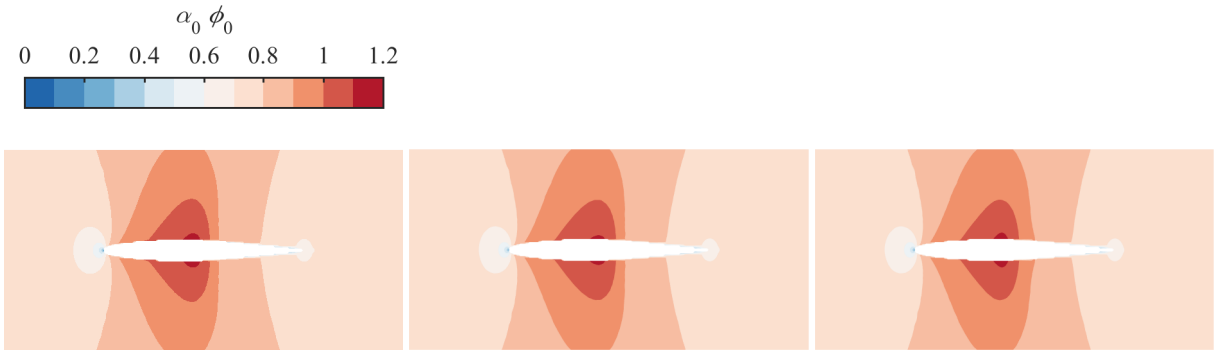

(a) $k = 0.1$. (b) $k = 0.3$. (c) $k = 0.5$.

Figure 7: Influence of the reduced frequency on the mean mode.

The Modal Assurance Criterion (MAC) is used in order to demonstrate quantitatively that the reduced frequency does not influence mode $\alpha_0\boldsymbol{\phi}_0$. The MAC is a technique used to compare mode shapes [14]. Considering two families of modes $\mathbf{x}^{\{1\}}$ and $\mathbf{x}^{\{2\}}$, the modal assurance criterion between the ith mode of the first family and the jth mode of the second family is calculated from

$$\mathrm{MAC}\left(\mathbf{x}_{(i)}^{\{1\}}, \mathbf{x}_{(j)}^{\{2\}}\right) = \left(\frac{\mathbf{x}_{(i)}^{\{1\}^{\mathrm{T}}} \mathbf{x}_{(j)}^{\{2\}}}{\left\|\mathbf{x}_{(i)}^{\{1\}}\right\| \left\|\mathbf{x}_{(j)}^{\{2\}}\right\|} \right)^2 . \tag{15}$$

A quantitative comparison is given by the value of the criterion, which varies between 0 and 1. If MAC is equal to 1, then the correlation is perfect. Figure 8 shows the MAC values calculated between the mean flow mode shapes $\alpha_0\boldsymbol{\phi}_0$ at the three values of k are always 1, which means that the modes are identical and that there is no effect of k on the mean mode shape.

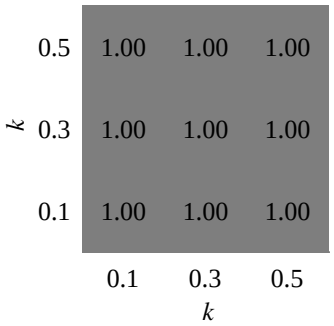

Figure 8: MAC matrix comparing the mean modes at different k.

Each dynamic mode is characterized by a spatial structure oscillating at a frequency $\Im(\lambda_i)$. The first dynamic mode given in Figure 9 oscillates at the fundamental frequency. Some streamlines have been added to better visualize the mode shape. The real part of the first dynamic mode has a vortex close to the trailing edge due to the pitching motion of the airfoil. Moreover, the streamlines around the airfoil indicate the expansion and contraction of the supersonic regions. However, it is difficult to give a precise physical interpretation of these streamlines because only the contribution of the first dynamic mode is illustrated.

Figure 9 also highlights that the first dynamic mode changes progressively as the reduced frequency k is increased. For instance, the MAC matrix points out that the mode shapes at $k = 0.1$ and $k = 0.5$ are quite different. The second dynamic modes, $\alpha_2\boldsymbol{\phi}_2$, obtained for different k

are even less correlated, as can be seen in Figure 10. As a result, the dynamics of the flow in time, and hence the variation of the shock positions, will also change with k. This analysis is consistent with the results shown for the shock motion in Figure 5.

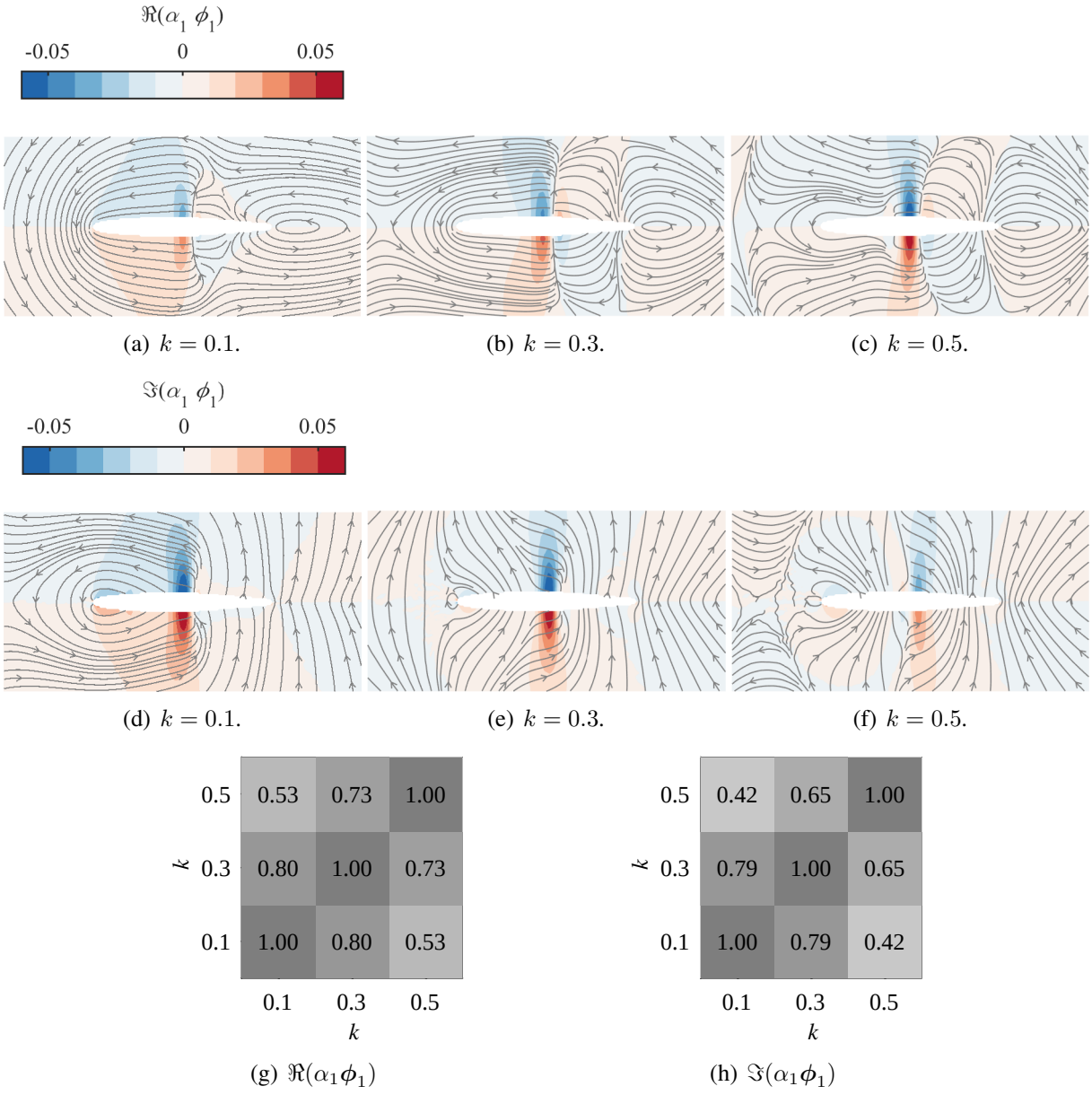

(a) $k = 0.1$. (b) $k = 0.3$. (c) $k = 0.5$.

(d) $k = 0.1$. (e) $k = 0.3$. (f) $k = 0.5$.

(g) $\Re(\alpha_1\phi_1)$ (h) $\Im(\alpha_1\phi_1)$

Figure 9: Influence of the reduced frequency on (a–c) the real part and (d–f) the imaginary part of DMD mode 1. MAC matrix that compares (g) the real part and (h) the imaginary part of DMD mode 1 at different k.

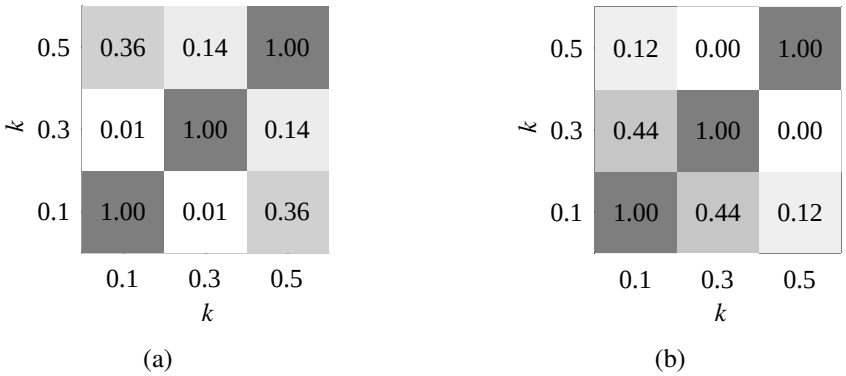

Figure 10: Influence of the reduced frequency on DMD mode 2. MAC matrix that compares (a) the real part and (b) the imaginary part of DMD mode 2 at different k.

The DMD analysis demonstrates that the frequency spectrum of the transonic flow around a pitching airfoil is discrete. It also allows the identification of the most dominant frequencies, which will be used with the Harmonic Balance (HB) method discussed in the following section.

5.2 Harmonic balance solutions

The transonic flow around the pitching airfoil is simulated with the harmonic balance method using the fundamental frequency of the flow, which is equal to the imposed pitching frequency. Another computation is carried out by adding the second harmonic. As discussed in the previous section, the DMD modes occur at the frequency of oscillation and its harmonics, exactly as in the case of a harmonic balance procedure with a single fundamental frequency. Therefore, a harmonic balance solution with only the fundamental frequency is a single-mode solution. If the second harmonic is included, the solution corresponds to a two-mode DMD representation.

Figure 11 shows the results for the aerodynamic forces and the shock motion. The results obtained with one mode are in good agreement with the time accurate unsteady solutions, especially for the aerodynamic forces. Two modes are sufficient to capture the time responses of the aerodynamic forces and the shock motion accurately. The HB computation for two input frequencies is significantly faster than a time-accurate computation. If the number of included frequencies increases, the estimations are more accurate, but the HB method can become expensive in terms of memory requirements and computation time.

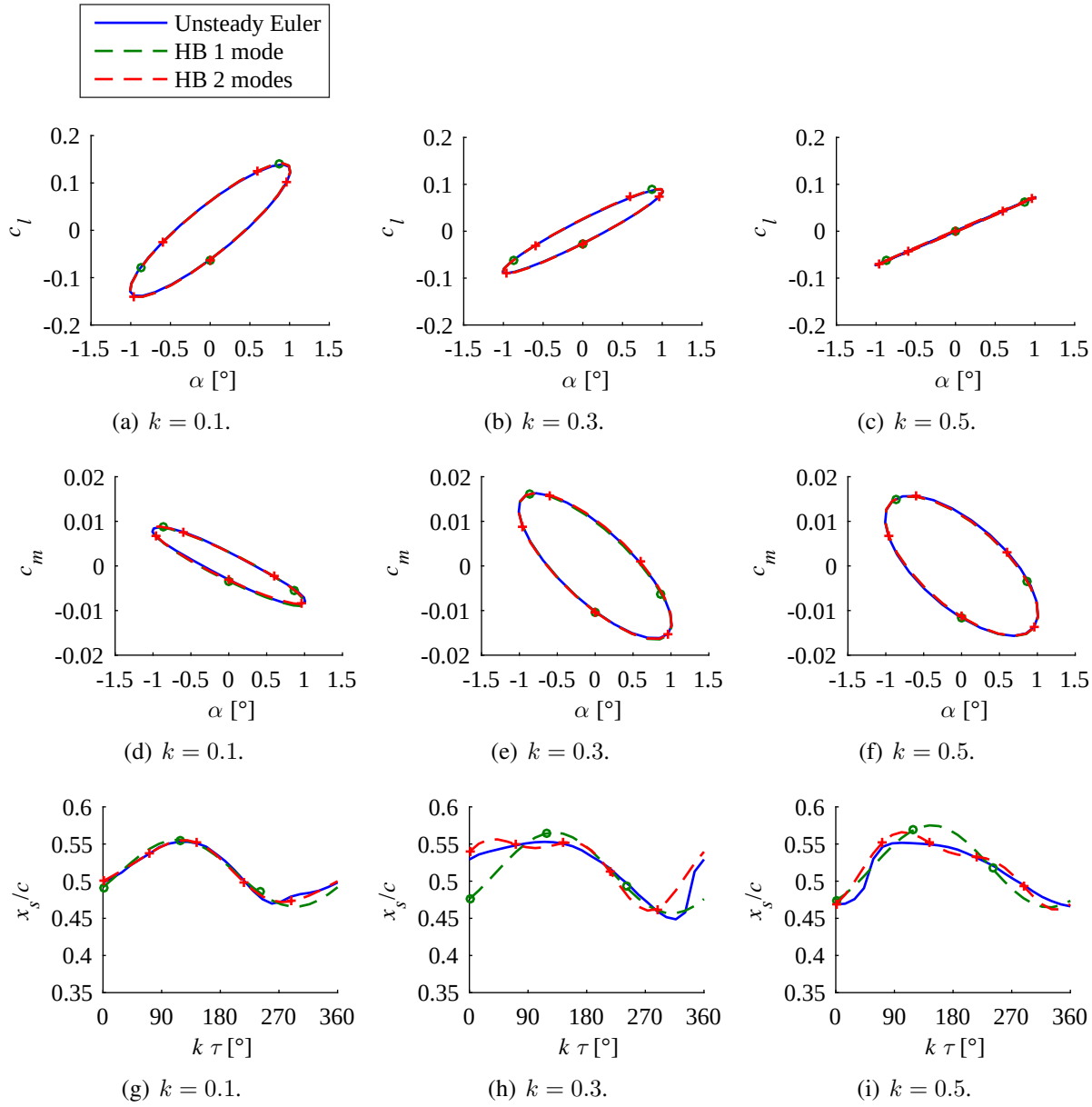

(a) $k = 0.1$. (b) $k = 0.3$. (c) $k = 0.5$.

(d) $k = 0.1$. (e) $k = 0.3$. (f) $k = 0.5$.

(g) $k = 0.1$. (h) $k = 0.3$. (i) $k = 0.5$.

Figure 11: Comparison between the results of unsteady simulations and harmonic balancing with 1 and 2 modes. Variation of (a–c) lift coefficient, (d–f) moment coefficient, and (g–i) position of the shock on the upper surface of the airfoil over one oscillation cycle, $k = 0.1$, 0.3, and 0.5.

5.3 Interpolation of dynamic modes

The previous analyses show that the dynamic behavior of the flow problem can be estimated by the most dominant modes. In this case, the relevant modes are essentially the first two dynamic modes. The idea of the proposed methodology is to compute the most dominant modes at several reduced frequencies, and then estimate the modes at an intermediate k by interpolation in order to take into account the modification of the mode shapes with k.

In the following example, the exact dynamic modes at $k = 0.3$ and $k = 0.5$ are used to estimate the dynamic modes at $k = 0.4$. The unsteady shock motion largely deviates from the one obtained by steady simulations at this intermediate reduced frequency (see Figure 5).

5.3.1 Mach field

The Mach field is first considered as it contains information about the moving shocks that can profoundly affect the aeroelastic instability. The related dynamic modes have been obtained by a harmonic balance simulation with two modes.

From a qualitative point of view, the first dynamic mode at $k = 0.4$ obtained using a linear interpolation of the exact modes at $k = 0.3$ and $k = 0.5$ is in good agreement with the exact solution at $k = 0.4$ as can be seen in Figure 12. Moreover, the MAC values given in Table 2 are very close to 1 indicating a very good correlation. Table 2 also shows that the interpolated second dynamic mode corresponds quite well to the exact solution.

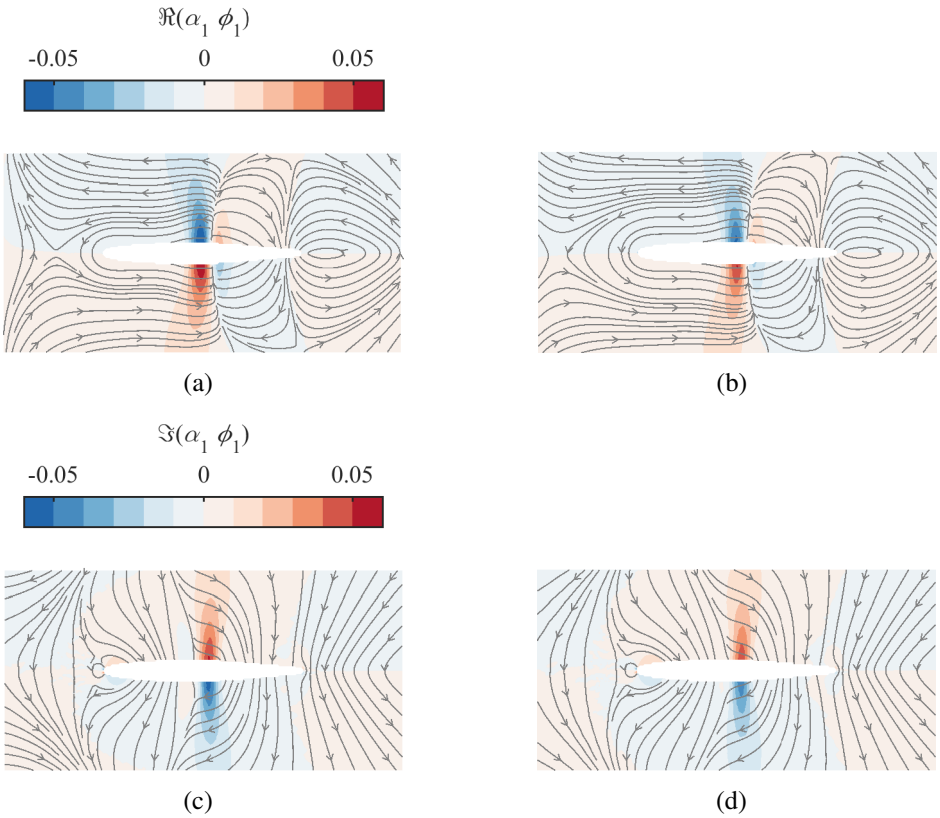

Figure 12: (a) Exact real part and (c) exact imaginary part of HB mode 1 at $k = 0.4$. (b) Real part and (d) imaginary part of HB mode 1 at $k = 0.4$ interpolated from the solution at $k = 0.3$ and $k = 0.5$.

	Mode 1		Mode 2	
	Real part	Imaginary part	Real part	Imaginary part
$k = 0.4$	0.99	0.98	0.87	0.85

Table 1: MAC values comparing the modes interpolated from a solution at $k = 0.3$ and $k = 0.5$ with the corresponding exact modes.

5.3.2 Pressure coefficient field

The pressure coefficient fields can also be considered in order to evaluate the aerodynamic lift and moment on the airfoil. Figure 13 reiterates the analysis of Figure 12 with the first dynamic mode associated with the pressure coefficient. Once again, the exact and interpolated mode shapes are very similar, as quantified in Table 13.

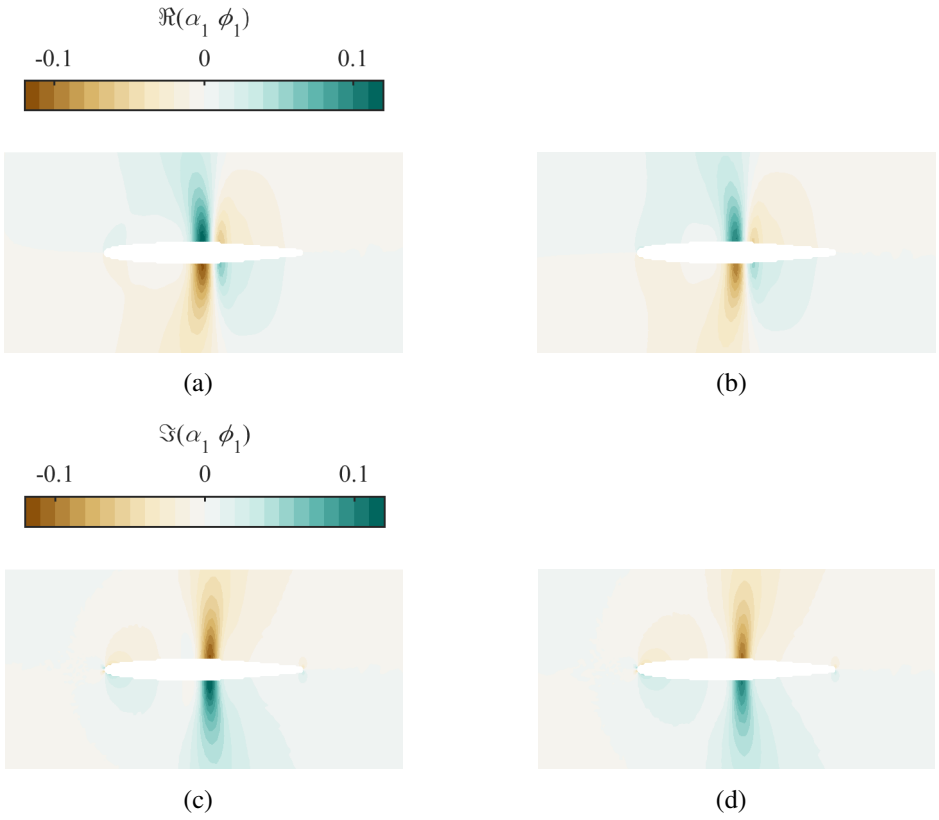

Figure 13: (a) Exact real part and (c) exact imaginary part of DMD mode 1 at $k = 0.4$. (b) Real part and (d) imaginary part of DMD mode 1 at $k = 0.4$ interpolated from $k = 0.3$ and $k = 0.5$.

	Mode 1		Mode 2	
	Real part	Imaginary part	Real part	Imaginary part
$k = 0.4$	0.99	0.98	0.87	0.85

Table 2: MAC values comparing the modes interpolated using $k = 0.3$ and $k = 0.5$ with the corresponding exact modes.

5.3.3 Lift, moment and shock motion

The evolution of the flow fields can be reconstructed from the interpolated modes. The aerodynamic lift and moment coefficients shown in Figure 14 are calculated from the pressure fields, and the shock motion is extracted from the Mach fields. The results obtained with the interpolated modes are in good agreement with the harmonic balance solutions.

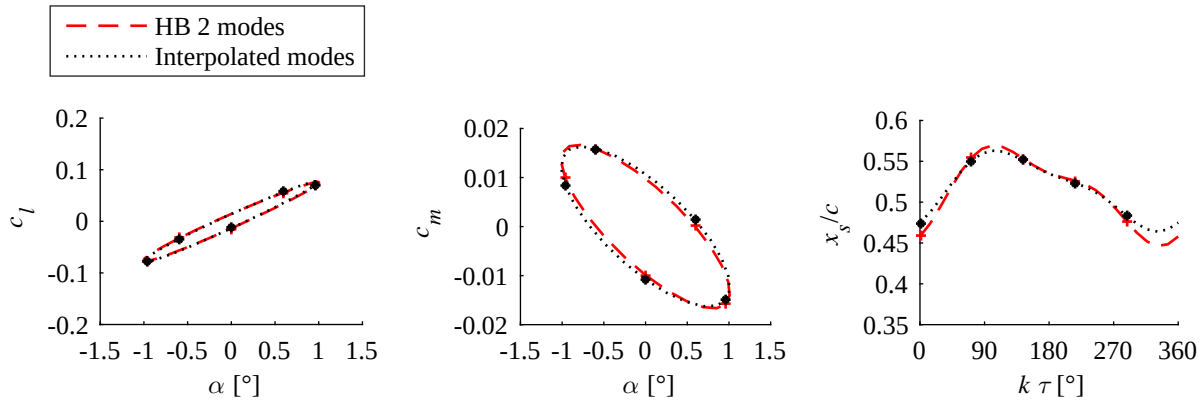

(a) Lift coefficient. (b) Moment coefficient. (c) Shock position.

Figure 14: Variation of (a) lift coefficient, (b) moment coefficient, and (c) position of the shock on the upper surface of the airfoil over one oscillation cycle, $k = 0.404$.

The first two dynamic modes can be estimated accurately for the range of reduced frequencies until $k = 0.5$ if the exact modes are available for $k = 0.1$, $k = 0.3$, and $k = 0.5$ as can be seen in Table 3. Table 4 shows that if the modes are interpolated from exact modes whose frequencies are further apart, i.e., $k = 0.1$ and $k = 0.5$, the first dynamic mode can still be estimated precisely by interpolation, but the second dynamic modes do not correlate well with the exact modes. In other words, this interpolation approach provides accurate results provided that the frequencies of the corresponding HB solutions are sufficiently close.

Overall, the second approach is more accurate than the first one, as it includes higher harmonics. However, its cost is also higher because it requires several HB simulations rather than simply two steady simulations.

	Mode 1		Mode 2	
	Real part	Imaginary part	Real part	Imaginary part
$k = 0.2$	0.97	0.99	0.82	0.92
$k = 0.4$	0.99	0.98	0.87	0.85

Table 3: MAC values comparing the modes interpolated using $k = 0.1$, $k = 0.3$, and $k = 0.5$ with the corresponding exact modes.

	Mode 1		Mode 2	
	Real part	Imaginary part	Real part	Imaginary part
$k = 0.2$	0.92	0.95	0.47	0.77
$k = 0.3$	0.87	0.88	0.09	0.44
$k = 0.4$	0.95	0.93	0.57	0.51

Table 4: MAC values comparing the modes interpolated using $k = 0.1$ and $k = 0.5$ with the corresponding exact modes.

6 CONCLUSIONS AND PERSPECTIVES

Applying an unsteady filter to a limited number of steady Euler solutions provides a first approximation of the transonic flow around a pitching airfoil. An advantage of relying on steady simulations is their independence with respect to frequency. Nevertheless, the shock motion becomes increasingly nonlinear as the frequency of the pitching airfoil increases, and this behavior cannot be fully recovered by applying the Theodorsen's filter. One research direction may be to develop an improved filter. On the other hand, instead of using this methodology as a stand-alone approach, it could be combined with a linear panel method so as to extend the range of applicability of the latter to transonic flows with moving shocks.

The dynamic mode decomposition of the unsteady Euler flow fields reveals that the flow dynamics can be represented by the most dominant dynamic modes. The first two dynamic modes, which can be obtained by a harmonic balance simulation, are sufficient to calculate the aerodynamic forces and the shock motion accurately in the case of a pitching airfoil. In addition, the dynamic modes can be estimated over an entire range of reduced frequencies by interpolation from the modes computed for a set of k values. In the present flow problem, interpolating from full solutions at $k = 0.1$, 0.3, and 0.5 provides accurate estimations of the first two dynamic modes for all $0 \leq k \leq 0.5$ and, hence, of the complete dynamic flowfields in this frequency range. This approach can significantly decrease the computational cost compared to repeated time-accurate simulations while accounting for the motion of the shocks. The formulation of the proposed approach still needs further development. In particular, different types of interpolation may be investigated.

Overall, both approaches represent a promising first step towards a fast and accurate transonic aeroelastic calculation methodology. Nonetheless, the present analysis is based on several simplifications. More specifically, a two-dimensional airfoil with only one degree-of-freedom has been considered. The two methods have relied on Euler simulations so that the nonlinear interaction between the shock and the viscous boundary layer cannot be captured. Finally, the pitching motion was restricted to small amplitudes. Future work will focus on extending the

present methodologies to more complex cases. Effort will also be directed towards the development of a new filter. Additionally, the present methodology will be illustrated in the case of a transonic flutter calculation.

7 ACKNOWLEDGEMENTS

The authors are grateful to the aerospace company Embraer S.A. for supporting this research.

8 REFERENCES

[1] Bendiksen, O. O. (2011). Review of unsteady transonic aerodynamics: theory and applications. *Progress in Aerospace Sciences*, 47(2), 135–167.

[2] Vio, G. A., Dimitriadis, G., Cooper, J. E., et al. (2007). Aeroelastic system identification using transonic CFD data for a wing/store configuration. *Aerospace Science and Technology*, 11(2), 146–154.

[3] Kalman, T., Rodden, W. P., and Giesing, J. (1971). Application of the doublet-lattice method to nonplanar configurations in subsonic flow. *Journal of Aircraft*, 8(6), 406–413.

[4] Chen, P.-C., Gao, X., and Tang, L. (2004). Overset field-panel method for unsteady transonic aerodynamic influence coefficient matrix generation. *AIAA journal*, 42(9), 1775–1787.

[5] Schmid, P. J. (2010). Dynamic mode decomposition of numerical and experimental data. *Journal of Fluid Mechanics*, 656, 5–28.

[6] Guissart, A., Andrianne, T., Dimitriadis, G., et al. (2013). Using proper orthogonal decomposition and dynamic mode decomposition methods for comparing cfd results and experimental measurements. In *Proceedings of the 16th International Forum on Aeroelasticity and Structural Dynamics*.

[7] Hall, K. C., Thomas, J. P., and Clark, W. S. (2002). Computation of unsteady nonlinear flows in cascades using a harmonic balance technique. *AIAA journal*, 40(5), 879–886.

[8] Da Ronch, A., McCracken, A. J., Badcock, K. J., et al. (2013). Linear frequency domain and harmonic balance predictions of dynamic derivatives. *Journal of Aircraft*, 50(3), 694–707.

[9] Economon, T. D., Palacios, F., Copeland, S. R., et al. (2015). Su2: An open-source suite for multiphysics simulation and design. *AIAA Journal*, 54(3), 828–846.

[10] Jovanović, M. R., Schmid, P. J., and Nichols, J. W. (2014). Sparsity-promoting dynamic mode decomposition. *Physics of Fluids*, 26(2), 024103.

[11] Nimmagadda, S., Economon, T. D., Alonso, J. J., et al. (2016). Robust uniform time sampling approach for the harmonic balance method. In *46th AIAA Fluid Dynamics Conference*. p. 3966.

[12] Davis, S. S. (1982). NACA 64A010 (NASA Ames model) oscillatory pitching. *AGARD Report*, 702.

[13] Fung, Y. C. (2002). *An introduction to the theory of aeroelasticity*. Courier Corporation.

[14] Allemang, R. and Brown, D. (1982). A correlation coefficient for modal vector analysis. In *Proceedings of the 1st International Modal Analysis Conference*. pp. 110–116.

COPYRIGHT STATEMENT